Hydroniumjarosite, $(H_3O)^+Fe_3(SO_4)_2(OH)_6$, from Cerros Pintados, Chile: Single-crystal X-ray diffraction and vibrational spectroscopic study

J. Plášil[1],*, R. Škoda[2], K. Fejfarová[1], J. Čejka[3], A. V. Kasatkin[4], M. Dušek[1], D. Talla[2,5], L. Lapčák[6], V. Machovič[6,7] and M. Dini[8]

[1] Institute of Physics ASCR, v.v.i., Na Slovance 2, Prague 8, CZ−182 21, Czech Republic
[2] Department of Geological Sciences, Masaryk University, Kotlářská 2, Brno, CZ−611 37, Czech Republic
[3] Department of Mineralogy and Petrology, National Museum, Cirkusová 1740, Prague 9, CZ−193 00, Czech Republic
[4] V/O "Almazjuvelirexport", Ostozhenka str., 22, block 1, 119034 Moscow, Russia
[5] Institut für Mineralogie und Kristallographie, Althanstraβe 14, 1090−Wien, Austria
[6] Institute of Chemical Technology, Prague, Technická 5, Prague 6, CZ−166 28, Czech Republic
[7] Institute of Rock Structures and Mechanics ASCR, v.v.i., V Holešovičkách 41, Prague 8, CZ−182 09, Czech Republic
[8] Pasaje San Agustin 4045, La Serena, Chile

ABSTRACT

The natural hydroniumjarosite sample from Cerros Pintados (Chile) was investigated by electron microprobe, single-crystal X-ray diffraction and vibrational spectroscopy (Infrared and Raman). The chemical composition of studied specimens (wt.%, mean of seven analyses) obtained from electron microprobe (in wt.%): Na_2O 1.30, K_2O 0.23, CaO 0.04, Fe_2O_3 50.49, Al_2O_3 0.37, SiO_2 0.33, SO_3 33.88, H_2O (calculated on the basis of $\Sigma(OH^- + H_3O^+)$ deduced from the charge balance) 13.32, total 99.98, corresponds to the empirical formula $(H_3O)^+_{0.77}(Na_{0.20}K_{0.02})_{\Sigma0.22}(Fe_{2.95}Al_{0.03})_{\Sigma2.98}$ $(OH)_{6.12}[(SO_4)_{1.97}(SiO_4)_{0.03}]_{\Sigma2.00}$ (calculated on the basis of S + Si = 2 a.p.f.u. (atoms per formula unit)). The studied hydroniumjarosite is trigonal, with space group $R\bar{3}m$, with $a = 7.3408(2)$, $c = 17.0451(6)$ Å and $V = 795.46(4)$ Å^3. The refined structure architecture is consistent with known jarosite-series minerals, including synthetic hydroniumjarosite. However, in the current study the presence of H_3O^+ is well documented in difference Fourier maps, where characteristic positive difference Fourier maxima, with apparent trigonal symmetry, were localized in the vicinity of the O4 atom in the channel-voids of the structure. The structure of natural hydroniumjarosite, including the H atoms, was refined to $R_1 = 0.0166$ for 2113 unique observed reflections, with $I_{obs} > 3\sigma(I)$. The present structure model, which includes the position of the H atom within the hydronium ion, is discussed with regard to the vibration spectroscopy results and earlier published density-functional theory (DFT) calculations for the alunite-like structure containing H_3O^+.

Introduction

THE minerals of the jarosite series (Bayliss *et al.*, 2010) involve a number of isostructural compounds, occurring mostly in acidic environments at surface or near-surface conditions. These minerals may be characterized by the general

formula $A_{1-x}(H_3O)_xFe_{3-y}^{3+}(SO_4)_2(OH)_{6-3y}$ $(H_2O)_{3y}$, where the A site is occupied by a monovalent (K, Na, H_3O^+, NH_4, Ag and Tl) or divalent (Pb) cation. In natural jarosite-group minerals, jarosite *sensu stricto*, natrojarosite and plumbojarosite, with dominant K, Na and Pb in the A site, respectively, are quite common, while hydroniumjarosite, ammoniojarosite, argentojarosite and dorallcharite with dominant H_3O^+, NH_4, Ag and Tl, respectively, should be considered as rare. The jarosite-group mineral that contains an elusive H_3O^+ group — hydroniumjarosite, was previously characterized in more detail by Majzlan *et al.* (2004). They provided the refined structure and thermodynamic properties for the synthetic phase. The structure elucidated from the neutron-powder diffraction and other physical properties was given by Bisson (2011). In this contribution, we provide a complex characterization of hydroniumjarosite with a natural origin for the first time. The presence of H_3O^+ was suggested during the microprobe study and is well supported by the refined structure from single-crystal X-ray diffraction (XRD) data and by Infrared (IR) and Raman spectroscopy. The natural specimen, as is commonly found, provides a more complex chemical composition, also involving an additional substitution at the A site.

Occurrence

The hydroniumjarosite specimen used in this study was collected in September 2010 by Maurizio Dini and Arturo Molina at the small sulfate outcrops, Cerros Pintados, Pampa del Tamarugal, Iquique Province, Tarapacá Region, Chile (20º47′26.79″S, 69º38′43.75″W). Cerros Pintados is the type locality for the sulfate minerals tamarugite (Schulze, 1889), pickeringite (Hayes, 1844) and cadwaladerite (Gordon, 1941).

The studied sample represents a 4.5 cm × 3.5 cm × 3 cm piece of matrix, which is covered by numerous brownish-orange transparent pseudohexagonal tabular crystals of hydroniumjarosite (Fig. 1).

Chemical composition

The chemical composition (Table 1) of the studied hydroniumjarosite crystal (the same as used for XRD study), was determined using a Cameca SX100 electron microprobe operating in the wavelength-dispersive mode with an accelerating voltage of 15 kV, specimen current of 4 nA and 8 μm beam diameter. The following X-ray lines and standards were selected to minimize line overlaps: Ca$K\alpha$ (wollastonite), Na$K\alpha$ (albite), Fe$K\alpha$ (andradite), K$K\alpha$, Al$K\alpha$ and Si$K\alpha$ (sanidine), S$K\alpha$ (synthetic $SrSO_4$). Peak counting times (CT) were $10-20$ s and the counting time for background was 50% of the peak CT. The measured intensities were converted to element concentrations using the *PAP* program (Pouchou and Pichoir, 1985).

The chemical composition of the crystals used for microprobe analysis is quite inhomogeneous (Table 1). However, in general, all the analysed points showed A-site deficiency in alkali cations and near-stoichiometric Fe_2O_3 concentration, suggesting that the B site is nearly fully occupied. The empirical formula of the studied hydroniumjarosite, calculated as the average of seven spot analyses on the basis of S + Si = 2 a.p.f.u., is $(H_3O)_{0.77}^+(Na_{0.20}K_{0.02})_{\Sigma 0.22}(Fe_{2.95}Al_{0.03})_{\Sigma 2.98}$ $(OH)_{6.12}[(SO_4)_{1.97}(SiO_4)_{0.03}]_{\Sigma 2.00}$. The H_3O^+ content was inferred so as to compensate the cationic deficiency at the A site. The OH content of the studied sample was inferred from the charge balance (see Discussion for further details).

Single-crystal XRD

An orange, 0.19 mm × 0.14 mm × 0.03 mm tabular crystal of hydroniumjarosite from the Cerros Pintados specimen was selected under the microscope for the single-crystal XRD experiment using an Oxford Diffraction Gemini four-circle single-crystal diffractometer. The
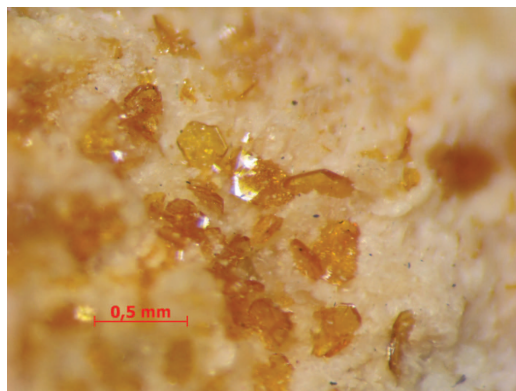

FIG. 1. Orange trigonal (pseudohexagonal) crystals of hydroniumjarosite growing on matrix. Photomicrograph A. Kasatkin.

TABLE 1. Chemical composition (from electron microprobe) of hydroniumjarosite from Cerro Pintados.

Wt.%	Mean	1	2	3	4	5	6	7
Na_2O	1.30	2.89	2.54	1.32	1.05	0.27	0.01	1.05
K_2O	0.23	0.51	0.62	0.20	0.14	0.00	0.00	0.15
CaO	0.04	0.18	0.00	0.00	0.00	0.12	0.00	0.00
Fe_2O_3	50.49	49.81	49.51	50.64	50.30	51.25	51.53	50.38
Al_2O_3	0.37	0.77	0.81	0.27	0.27	0.00	0.16	0.31
SiO_2	0.33	0.33	0.31	0.44	0.29	0.31	0.27	0.37
SO_3	33.88	34.05	33.47	34.20	33.93	33.59	34.20	33.74
Subtotal	86.64	88.54	87.26	87.07	85.98	85.54	86.17	86.00
H_2O^*	13.32	13.29	13.28	13.24	13.22	13.43	13.55	13.25
Total	99.98	101.83	100.54	100.31	99.20	98.97	99.72	99.25
a.p.f.u.								
Na_2O	0.196	0.433	0.387	0.196	0.158	0.041	0.001	0.158
K_2O	0.023	0.050	0.062	0.020	0.014	0.000	0.000	0.015
CaO	0.004	0.015	0.000	0.000	0.000	0.010	0.000	0.000
ΣA site	0.223	0.498	0.449	0.216	0.172	0.051	0.001	0.173
FeO	2.990	2.896	2.930	2.919	2.940	3.023	2.990	2.951
Al_2O_3	0.034	0.070	0.075	0.024	0.025	0.000	0.015	0.028
ΣB site	3.024	2.966	3.005	2.943	2.965	3.023	3.005	2.979
SiO_4	0.026	0.024	0.024	0.034	0.023	0.024	0.021	0.029
SO_4	1.974	1.976	1.976	1.966	1.977	1.976	1.979	1.971
ΣT site	2.000	2.000	2.000	2.000	2.000	2.000	2.000	2.000
H_3O^+	0.774	0.502	0.550	0.784	0.828	0.949	0.999	0.827
OH	6.119	6.346	6.417	5.980	6.020	6.070	5.974	6.055

Mean − average composition on 1−7 point analyses
* H_2O − content in wt.% calculated on the basis of $\Sigma(OH^-+H_3O^+)$ deduced from the charge balance.
Coefficients of empirical formula calculated on the basis of (S + Si) = 2 a.p.f.u.

MoKα radiation (λ = 0.71073 Å), from a sealed X-ray tube was monochromatized with a graphite monochromator, collimated with a fibre optics Mo-Enhance collimator and detected with an Atlas CCD detector. Omega rotational scans, with a frame width of 0.8º and a collection time of 35 s per frame, were used to assemble the three-dimensional intensity data. The unit cell was refined from 2825 reflections, which provided $a = 7.3408(2)$, $c = 17.0451(6)$ Å with $V = 795.46(4)$ Å^3. Diffraction frames did not reveal any additional reflections that might arise from the twinning of the crystal. Of the 3841 reflections collected, 2393 were unique and 2113 classified as observed [$I_{obs}>3\sigma(I)$]. The data were corrected for background, Lorentz effect and polarization using *CrysAlis RED* (Agilent Technologies, 2012). A combination of analytical (after Clark and Reid, 1995) and multi-scan absorption correction, $\mu = 4.54$ mm^{-1}, was applied (*CrysAlis RED*, Agilent Technologies 2012),

leading to the data set with $R_{int} = 0.029$. The details for the data collection and refinement are listed in Table 2.

The crystal structure (Tables 3, 4) was solved by the charge-flipping algorithm implemented in the *Superflip* program (Palatinus and Chapuis, 2007) and subsequently refined by the full-matrix least-squares algorithm based on F^2 using the *JANA2006* program (Petříček *et al.*, 2006). The space group $R\bar{3}m$ was chosen based on the reflection conditions. The space group is in accordance with the previously published structure reports (Hendricks, 1937; Wills and Harrison, 1996; Majzlan *et al.*, 2004) and it was also confirmed by the *Superflip* output (Palatinus and van der Lee, 2008). All atoms, except the H atoms, were refined aniso-tropically. The H atom of the OH group was found from the difference Fourier maps in the vicinity of the O3 atom and was refined with the soft restraint that the O−H bond be 0.78 Å (with a weight constraint set to 0.02) and the U_{iso} be equal to

TABLE 2. Data collection and refinement details for hydroniumjarosite from Cerro Pintados.

Structural formula	$(H_3O)Fe_{2.911}(SO_4)_2(OH)_6$
Space group	$R\bar{3}m$
a, c (Å) (from 2825 reflections)	7.3408(2), 17.0451(6)
V (Å^3)	795.46(4)
Z	3
D_{calc} [g cm^{-3}]	2.970
Temperature	300 K
Wavelength	Mo$K\alpha$, 0.7107 Å
Crystal dimensions (mm)	$0.19 \times 0.14 \times 0.03$
Collection mode, frame width, counting time	ω scans, 0.8°, 35 s
Limiting θ angles	3.4−29.3°
Limiting Miller indices	−9<h<9, −9<k<9, −21<l<22
No. of reflections	3841
No. of unique reflections	2393
No. of observed reflections (criterion)	2113 [$I_{obs}>3\sigma(I)$]
Absorption coefficient (mm^{-1})	4.539; 0.563/0.881
R_{int}; completeness up to θ max	0.029; 99.74%
F_{000}	703
Refinement by *Jana2006* on F^2	
No. parameters, restraints, constraints	31, 2, 1
R_1, wR_2 (obs)	0.0166, 0.0529
R_1, wR_2 (all)	0.0180, 0.0534
GOF obs/all	2.03/2.08
Weighting scheme, details	$\sigma, w = 1/(\sigma^2(I) + 0.0004I^2)$
$\Delta\rho_{min}, \Delta\rho_{max}$ (e/Å^3)	−0.44, 0.15

$1.2 \times U_{eq}$ of the parent (donor) O atom. The position of the difference-Fourier maximum, which corresponds with the position of the H atom of the H_3O^+, was introduced into the structure model and subsequently refined. The symmetry operation of the three-fold screw axis, applied to the new atomic site H2 (Wyckoff site 18*h*; the full site occupancy equal to 0.5), generates the six possible positions of the H atoms. The following distinct approaches to the refinement were chosen in order to examine the behaviour of the refined values for the thermal displacement parameter of the H2 atom: (1) H2 treated as the fully occupied site in order to test sensitivity of the refined U_{iso} (H2) to this incorrectly (for a crystal-chemical reason) assigned occupancy; (2) occupancy of the H2 site set to 0.50 (then producing 3 H atoms for $Z = 3$), while the partial occupancy of the *A* site by

TABLE 3. Atom fractional coordinates and equivalent displacement parameters (in Å^2) for hydroniumjarosite.

Atom	Occ.	x	y	z	U_{eq}
Fe	0.970(4)	0.333333	0.166667	0.166667	0.00950(19)
S		0.666667	0.333333	0.02556(5)	0.0107(3)
O1		0.666667	0.333333	−0.06013(15)	0.0157(6)
O2		0.4472(2)	0.22362(12)	0.05494(8)	0.0157(5)
O3		0.12726(13)	0.2545(3)	0.13504(10)	0.0172(6)
O4		0	0	0	0.0229(11)
H1		0.1752(15)	0.350(3)	0.1094(16)	0.0206*
H2	0.5	−0.053(3)	0.053(3)	−0.036(2)	0.046(19)*

* Treated with U_{iso}; all other atoms were refined anisotropically; U_{eq} is defined as a third of the trace of the orthogonalized U_{ij} tensor.

TABLE 4. Anisotropic displacement parameters for hydroniumjarosite (in Å^2).

Atom	U^{11}	U^{22}	U^{33}	U^{12}	U^{13}	U^{23}
Fe	0.0074(3)	0.0098(2)	0.0105(3)	0.00368(13)	0.00027(13)	0.00014(7)
S	0.0119(3)	0.0119(3)	0.0082(4)	0.00594(16)	0	0
O1	0.0190(8)	0.0190(8)	0.0090(11)	0.0095(4)	0	0
O2	0.0108(8)	0.0209(6)	0.0120(7)	0.0054(4)	0.0007(5)	0.0003(3)
O3	0.0101(6)	0.0133(8)	0.0293(9)	0.0066(4)	0.0048(3)	0.0097(7)
O4	0.0263(14)	0.0263(14)	0.016(2)	0.0131(7)	0	0

Na^+ was ignored; (3) occupancy of the site refined along with the U_{iso} of the H2 atom. The results of the refinement, including the distinct refined position of the H2 atom, thermal displacement parameters, residuals of the refinement and difference-Fourier densities are listed in Table 5. The final solution retained was (2), which converged with the residuals $R_1 = 0.0166$ and $wR_2 = 0.0529$, with a GOF = 2.08 for unique observed reflections (Table 2). The decrease in R values, GOF and the difference-Fourier electron density provide convincing evidence that the model, including positions of the H atom within the H_3O^+, better describes the observed electron density. The final composition, resulting from the selected model can be expressed by the formula $(H_3O)^+Fe_{2.911}(SO_4)_2(OH)_6$, which is not electro-neutral, however, here, this is just a consequence originating from the chosen approach to the refinement. The discussion covering the relevancy of the structure model follows below in greater detail. The bond-valence analysis, based on interatomic distances (Table 6) of the hydroniumjarosite structure was carried out after Brown (2002) (for details see Table 7). Graphical visualization of the electron density was performed by *Vesta* software (Momma and Izumi 2008). The cif files along with the list of reflections are deposited with the Principal Editor of *Mineralogical Magazine* and are available from www.minersoc. org/pages/e_journals/ dep_mat_mm.html.

General structure architecture

The crystal structure of the studied hydroniumjarosite is similar to the results presented previously by Wills and Harrison (1996), Majzlan *et al.* (2004) or Bisson (2011) for the synthetic analogues and also similar to the principal features of the jarosite-group minerals as determined by Hendricks (1937) or Sato *et al.* (2009). The structure of hydroniumjarosite consists of sheets of $Fe\Phi_6$ (Φ = miscellaneous ligands) octahedra decorated by sulfate tetrahedra. The Fe(III) ions are positioned on a triangular Kagomé lattice (Fig. 2) and this triangular arrangement gives rise to the specific magnetic properties of jarosite (Majzlan *et al.*, 2004; Nocera *et al.*, 2004; Grohol and Nocera, 2007; Majzlan *et al.*, 2010).

TABLE 5. Results of the structure refinement including the H2 atom of the H_3O^+ group.

	Occ.	U_{iso} (H2)	R_1, wR_2 (all)/GOF all	$\Delta\rho_{min}$, $\Delta\rho_{max}$ (e/Å^3)
(1)	1.00	0.55(13)	0.0179, 0.0567/2.16,	−0.48/0.19
(2)	**0.50**	**0.045(19)**	**0.0180, 0.0534/2.03**	**−0.44/0.15**
(3)	0.46(4)	0.040(26)	0.0181, 0.0529/2.02	−0.48/0.16

Occ. − Refined occupancy of the site
Fractional coordinates for H2 atom (x, y^*, z):
(1) −0.034(18), 0.034(18), −0.050(6)
(2) −0.0527(30), 0.0527(30), −0.0364(24)
(3) −0.0534(38), 0.0534(38), −0.0376(30)
* Symmetry restriction

TABLE 6. Selected interatomic distances and H-bond geometry for hydroniumjarosite.

Fe−O2	2.0387(15)	S−O1	1.462(3)	
Fe−O2^i	2.0387(15)	S−O2	1.4818(17)	
Fe−O3	1.9921(19)	S−O2^{iv}	1.482(2)	
Fe−O3^{ii}	1.9922(11)	S−O2^v	1.4818(17)	
Fe−O3^{iii}	1.992(3)	<S−O>	1.478	
Fe−O3^i	1.9921(18)			
<Fe−O>	2.008			
	D−H	H⋯*A*	*D*⋯*A*	<*D*−H⋯*A*>
O3−H1⋯O1^{vi}	0.75(2)	2.17(2)	2.915(2)	171(3)
O4−H1⋯O3	0.91(3)	1.93(4)	2.814(2)	162(3)

Symmetry codes: (i) −*x*+2/3, −*x*+*y*+1/3, −*z*+1/3; (ii) −*x*+*y*, −*x*, *z*; (iii) *x*−*y*+2/3, −*y*+1/3, −*z*+1/3; (iv) −*y*+1, *x*−*y*, *z*; (v) −*x*+*y*+1, −*x*+1, *z*; (vi) *y*, *x*, −*z*.

A H atom is bonded to the O3 atoms at the shared vertex between two FeΦ$_6$ octahedra, thus providing the linkage between adjacent (FeΦ$_6$−SO$_4$) sheets through the O3−H1⋯O1 bonds (Fig. 3). The monovalent metal cations and/or H$_3$O$^+$ occupy the interlayer positions in the structure (special position 3*a* with corresponding coordinates 0, 0, 0). According to bond-valence analysis, this O atom should actually belong to a H$_2$O molecule; however, it is clear, that it represents an H$_3$O$^+$ ion, due to the overall balance of the charge and the characteristic features of H$_3$O$^+$, described below. The direct elucidation of the remaining H atoms from the difference Fourier maps is not straightforward, as also observed by Majzlan *et al.* (2004). Who, after Wills and Harrison (1996), stated that lowering the $R\bar{3}m$ symmetry is necessary to describe the disorder of the H atoms in the H$_3$O$^+$ group.

Elucidation of the H$_3$O$^+$ group from single-crystal XRD

All significant difference-Fourier maxima, which belong to the H atoms of the H$_3$O$^+$ group, were located in the vicinity of the O4 atom, at the special position (0, 0, 0). The difference-Fourier electron density on Fig. 4*b* apparently reflects trigonal symmetry, belonging to the distribution of the H atoms in the H$_3$O$^+$ group. The two orientations of the electron density in Fig. 4*b* suggest that there may be a dynamic disorder, including hopping of the proton over the disordered sites, similar to that observed in synthetic hydroniumjarosite at 4.2 K using powder diffraction at neutron source (Bisson, 2011). Such behaviour should also be apparent from the refined values of atomic displacement parameters of particular H atoms.

TABLE 7. Bond-valence analysis for the structure of hydroniumjarosite.

	O1	O2	O3	O4	ΣBV
Fe		0.47 × 2→	0.53 × 2↓, × 4→		3.07
S	1.55	1.47 × 3→			5.95
H1	0.18 × 3↓		0.83		1.01
H2			0.24	0.70 × 3↓	0.94
ΣBV	2.10	1.94	2.13	2.10	

Values are expressed in valence units (vu). ΣBV, bond-valence sums; ×2↓, multiplicity; Na4 atom was not included in the BV calculations. Bond-strength parameters were taken from Brown and Altermatt (1985) (Fe−O bond), Brese and O'Keeffe (1991) (S−O bond), and Brown (2002) (H−O bond strength).
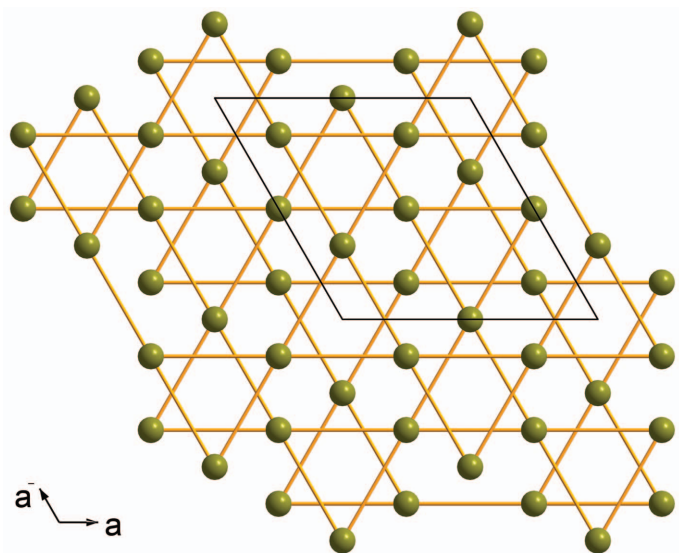
FIG. 2. Kagomé-net lattice in the structure of hydroniumjarosite arising from the distribution of Fe(III) ions (green). Unit-cell edges are outlined by the solid black line.

The trigonal symmetry of the difference Fourier maximum is indeed forced by the symmetry used for the calculation of the Fourier map. The weakness of the diffraction signal from oxonium's H atoms does not allow the maxima to be seen in a map calculated using $P1$ symmetry. However, the trigonal symmetry has been proven for our crystal structure (R_{int} of the dataset) and there is no reason to assume that only the H atom of the H_3O^+ ion would break it. If it was broken,
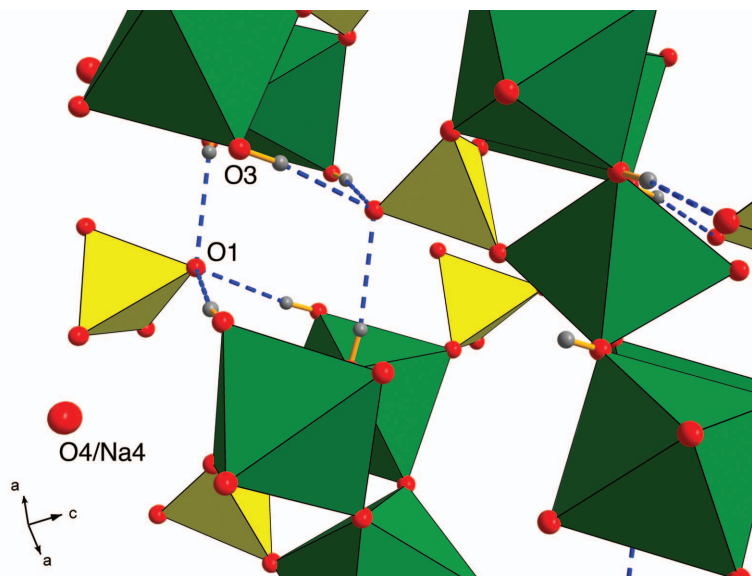
FIG. 3. Detail of the H bonds of the OH groups in hydroniumjarosite. The H bond of the H1 atom (grey) is accepted by the O1 atom of the SO_4 tetrahedra. Each O1 atom receives three H bonds from adjacent FeO_6 octahedra.
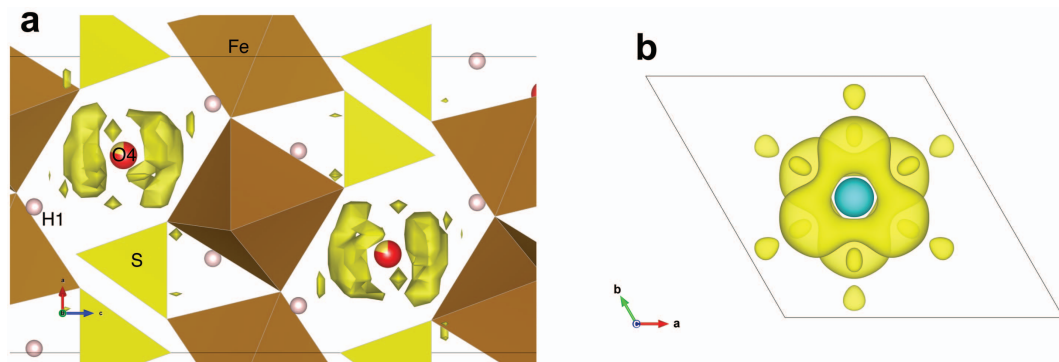
F<small>IG</small>. 4. Difference-Fourier electron density in the vicinity of the O4/Na4 atom. (*a*) View of the part of hydroniumjarosite structure, where the significant maxima of the positive difference electron density is located only around the O4/Na4 atom. (*b*) The 3D projection of the difference Fourier electron density along *z*. The two groups of maxima have trigonal symmetry, above and below the O4/Na4 atom (blue).

the additional maxima would also be enhanced and reproduced by the three-fold symmetry, which was not observed in our case. Moreover, the final refined H positions (see later) have a very good fit with the difference maxima.

Infrared and Raman spectroscopy

For the IR spectroscopic measurements, the sample was diluted in KBr in a weight ratio sample/KBr = 1:300 and processed into pellets 1 mm thick. The dilution was necessary, even for the small amount of sample used, due to the strong OH$^-$ and fundamental absorption bands. The pellet was then measured using a Bruker Tensor27 IR spectrometer (Globar light source, KBr beam splitter, DTGS detector) with a spectral resolution of 4 cm^{-1}. The background spectrum was scanned using a blank KBr pellet. The actual measurement was averaged over 100 individual scans to suppress high noise and enhance the quality of the result.

The Raman spectrum of the hydroniumjarosite single crystal (the same as studied by XRD) was collected using a DXR dispersive Raman spectrometer (Thermo Scientific) on a confocal Olympus microscope with a $100 \times$ objective in the range 50−4000 cm^{-1} at a spectral resolution of 2 cm^{-1}. The Raman signal was excited by a 532 nm diode-pumped solid-state laser and detected by a CCD detector. Exposure time: 10 s; number of exposures: 32; grating: 400 lines per mm; spectrograph aperture: 50 mm slit; camera temperature: 50ºC; laser power: 3.0 mW; and CCD detector. The instrument was calibrated by a software-controlled calibration procedure using multiple Ne emission lines (wavelength calibration), multiple polystyrene Raman bands (laser frequency calibration) and standardized white light sources (intensity calibration). Spectral data were processed using *OMNIC Spectral tool software v.7.3* (ThermoElectron Corp.).

Infrared and Raman spectra of hydroniumjarosite (Fig. 5*a* and *b*) were interpreted following the papers by Kubisz (1968), Ross (1974), Wilkins *et al.* (1974), Nakamoto (1986), Serna *et al.* (1986), Sasaki *et al.* (1998), Čejka (1999), Frost *et al.* (2006), Lane (2007), Murphy *et al.* (2009), Chio *et al.* (2010), Gale *et al.* (2010), Majzlan *et al.* (2011) and Spratt *et al.* (2013). The overview of the wavenumbers and tentative assignments is listed in Table 8.

Both IR and Raman spectra are dominated by O−H stretching and SO$_4$ stretching vibrations. The O−H stretching region (~3700 to ~2100 cm^{-1}) is composed of the overlapping stretching vibrations from OH, H$_2$O and also H$_3$O$^+$ groups. The vibrations at the largest wavenumber belong, according to Libowitzky′s relation (Libowitzky, 1999), to the weak H bond (>3.2 Å). The separation O···O distances of corresponding H bonds in the structure of hydroniumjaroisite, inferred from the above mentioned empiric relation given by Libowitzky (1999), vary in the range 2.6−3.2 Å. These distances match the range calculated from the refined structure model (Table 6). The spectral region 1600−1750 cm^{-1} is interesting in this context, where H$_2$O bending modes occur. In the case of hydroniumjarosite, which is nominally
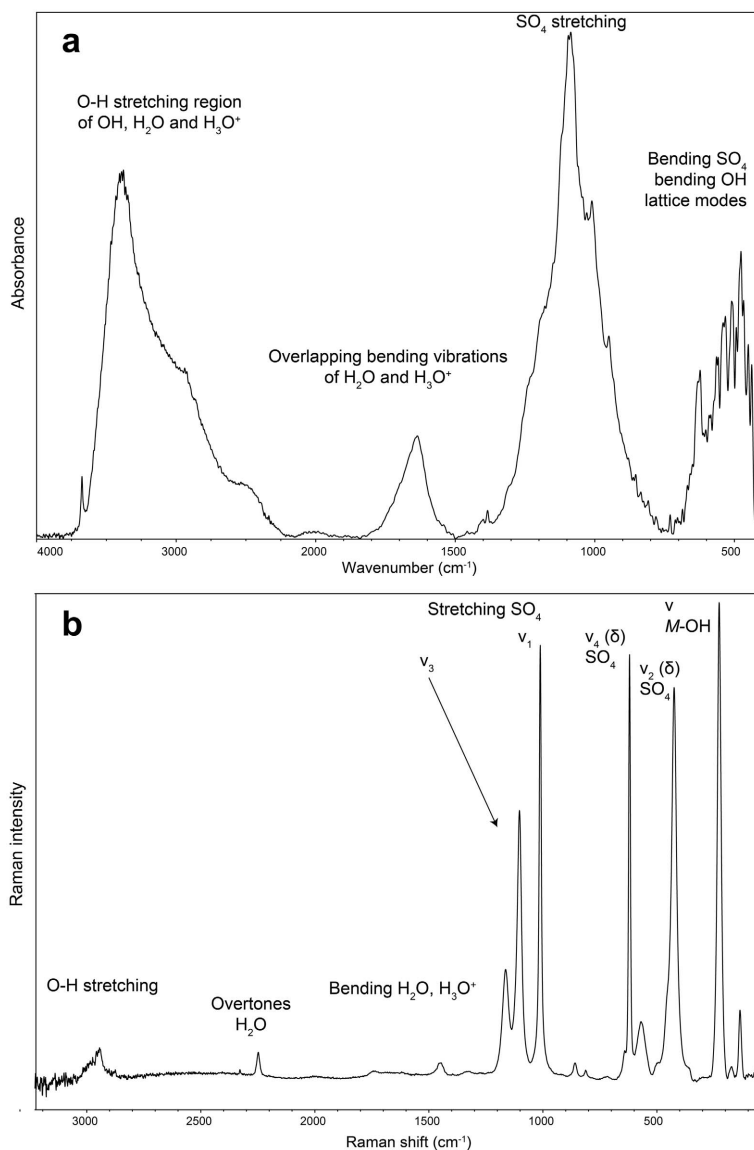
FIG. 5. Infrared and Raman spectra of hydroniumjarosite.

anhydrous, the region is dominated by a broad band of overlapping vibrations, including the H_3O^+ bending (IR at 1715 cm^{-1} and Raman at 1742 and 1687 cm^{-1}) and the H_2O bending (IR at 1640 cm^{-1} and Raman at 1622 cm^{-1}). The presence of these bands supports the presence of H_2O molecules in the structure of the studied sample (see Discussion below). It is also worth noting that Gale *et al.* (2010) calculated the phonon spectrum for hydronium alunite and

provided two wavenumbers (1627 and 1602 cm^{-1}) for the pure bending modes of H_3O^+.

Discussion

The water content in hydroniumjarosite

The water content in hydroniumjarosite is somewhat elusive and this issue is worthy of comment. The generally accepted formula for minerals of the jarosite series, $A_{1-x}(H_3O)_x Fe_{3-y}^{3+}$

TABLE 8. Infrared and Raman spectra of hydronium-jarosite: frequencies (in cm^{-1}) and assignments.

Infrared	Raman	Assignment
3680		
3410		
3190		
	2989	O−H stretching
2940	2945	
	2878	
2500		
	2328	Combination bands (H$_2$O)
	2248	and overtones (SO$_4$)
2030	2002	
1715	1742	
	1678	Overlapping bending
1640	1622	modes of H$_2$O and H$_3$O$^+$
1550		
	1477	(SO$_4$) overtones
	1449	
1300	1329	
1245		δ OH
1190		
1165		ν_2 H$_3$O$^+$?
1120	1103	
1085		ν_3 (SO$_4$)
1015	1012	
970		ν_1 (SO$_4$)
	859	
	812	δ OH
	722	
	643	
620	620	ν_4 (δ) (SO$_4$)
585		
565	569	
530		δ OH, ν Fe−O
510		
490	497	
480		ν_2 (δ) (SO$_4$)
465		
450	454	
	424	
	367	ν M–OH
	227	
	172	
	135	Lattice modes
	62	

(SO$_4$)$_2$(OH)$_{6-3y}$(H$_2$O)$_{3y}$, suggests that the H$_2$O content is connected to the occupational disorder at the Fe^{3+} site and the H$_3$O$^+$ content balances the deficiency at the A site, occupied nominally by monovalent (K, Na, Ag, Rb, NH$_4$, Tl) and divalent (Pb) cations (Dutrizac and Jambor, 2000; Bayliss et al., 2010). Majzlan et al.

(2004) mentioned, however, that H$_3$O$^+$ might play a lesser role in the structures than is commonly assumed (for cation-deficient analysis of the jarosite compounds), as the A position need not be fully occupied. They refined the structure of a compound with the nominal composition (H$_3$O)$_{0.91}$Fe$_{2.91}$(SO$_4$)$_2$[(OH)$_{5.64}$(H$_2$O)$_{0.18}$], inferred from the structure refinement results (A-site occupancy) and chemical analysis. The IR spectrum they published also clearly shows the presence of bending vibrations of the molecular H$_2$O and H$_3$O$^+$. In further studies of jarosite and alunite-group compounds (Majzlan et al., 2010; Nielsen et al., 2007, 2008, 2011), a number of well characterized synthetic compounds were examined by various techniques of solid-state NMR. Nielsen et al. (2011) concluded that H$^+$ ions in H$_3$O$^+$ groups (or D$_3$O$^+$) at the A site do not react with the OH groups within the framework, distinguishing the distinct resonances attributable to FeO(D)−Fe, Fe−OD$_2$ and D$_3$O/D$_2$O local environments. Based on those spectra, they excluded the previously postulated reaction mechanism based on the interaction of the H$_3$O$^+$ and OH$^-$ resulting in H$_2$O formation (Grohol and Nocera, 2007; Grohol et al., 2003) and proposed another mechanism, which involves the formation of M^{3+} (Fe or Al) vacancies at the B site and the formation of terminal OH$_2$ (OD$_2$) groups.

Our sample brings yet another complication into this already rather complex group of phases. It is characterized by a homogeneous non-deficient B site (Fe + Al contents) (see Table 1) and a deficient A site, occupied, besides the O atom of the H$_3$O$^+$, by Na$^+$ (up to 0.43 a.p.f.u.). There is certainly some degree of H$_3$O$^+$/H$_2$O dynamic disorder at the A site and some minor H$_2$O may also be present within the framework. The B site deficiency is unusually low, however, and the vacancies are probably distributed stochastically within the crystal.

The orientation of the H$_3$O$^+$ in the alunite-group minerals structures: Diffraction techniques vs. DFT

The elucidation of the exact position, orientation and the nature of the H$_3$O$^+$ in the structure of the alunite mineral supergroup were the subjects of the research for which various non-diffraction techniques were used (e.g. Ripmeester et al., 1986; Breitinger et al., 1997; Lager et al., 2001; Nielsen et al., 2007, 2008, 2011). The question of the nature of the H$_3$O$^+$ within alunite-like

structures, i.e. if the group has a static character or if it is rotating and re-orientating within the voids in the structures, was partially answered by Nielsen *et al.* (2007), who proposed a complex motional averaging connected with the rotation about multiple axes, breaking the symmetry of the $\bar{3}$ rotational axis. Gale *et al.* (2010) used first-principles (*ab initio*) quantum calculations to discover the behaviour of H_3O^+ in the alunite crystal structure. Their results showed that H_3O^+ differs from the orientation proposed earlier by Basciano and Peterson (2007) in which the three-fold rotational symmetry of both the isolated H_3O^+ and the cationic *A* site are aligned. The quantum calculations showed that the hydronium ion prefers to rotate such that the plane of the three H atoms is closer to being parallel to the *c* axis than to the *a−b* plane of the alunite unit cell. It forms two H bonds to the OH groups and one bond linking the O atom of the SO_4 group. Gale *et al.* (2010) proposed further that the energetic driver for the orientation change of the hydronium ion must be the lower strength of the H bond to the SO_4 group than to an OH group. According to the calculations the corresponding distances for the H···OH and H···OSO_3 interactions are in the ranges 1.550−1.720 and 1.818−1.901 Å, respec-

tively (depending on the functional used for *ab initio* calculations). Further, Gale *et al.* (2010) concluded that due to the preference for adopting such a tilted orientation, the H_3O^+ is then able to occupy 12 symmetrically distinct configurations within each *A* site with the same combination of H bonds. This leads to a greater entropic stabiliza-tion and to the scatter of electron density (disorder), which they concluded, (Gale *et al.*, 2010), is too large to locate adequately the H atoms by diffraction techniques. These results should be considered when discussing the nature of the H_3O^+ in hydroniumjarosite.

Our structure model reveals that H_3O^+ forms three H bonds to the O3 atom of the OH group (Fig. 6). As stated above, Gale *et al.* (2010) proposed two of the H atoms within hydronium links by H bonds to these O atoms. It is also reasonable when looking at the bond-valence sum for the O3 site, which is slightly undersaturated, as the contribution from the H bond would saturate it. The small oversaturation of the corresponding O site (O3 in our model) is probably compensated by the highly dynamic nature of the system. The calculated geometry for the O4−H2···O3 bond is listed in Table 7. The information about the H_3O^+ ion provided here by
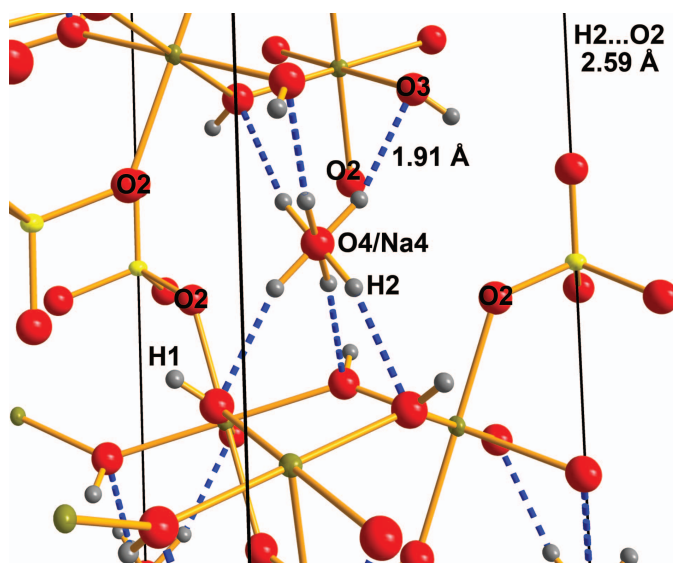

FIG. 6. Detailed view of the position and environment of the H_3O^+ group obtained from the final refinement. The six O4−H2···O3 hydrogen bonds, from all possible orientations of the H2 atom given by the model, are displayed as blue dashed lines. The interatomic distance between H2 (proposed by the current model) and O2 atom of the SO_4 tetrahedron is given at the top right. This O atom is proposed by Gale *et al.* (2010) to be linked by H bonds to the hydronium ion. The *c* axis is parallel with the unit-cell edges outlined as the solid black lines.

current structure determination, based on the single-crystal XRD data (Fig. 6), should probably be considered as the maximum, which is recoverable from the diffraction data and provides similar results to the neutron powder diffraction data (Bisson, 2011). For finer details of the behaviour of the hydronium ion only the non-diffraction time-resolved techniques should be used.

Acknowledgements

References

Agilent Technologies (2012) *CrysAlis CCD and CrysAlis RED*. Oxford Diffraction Ltd, Yarnton, UK.

Basciano, L.C. and Peterson, R.C. (2007) Jarosite-hydronium jarosite solid-solution series with full iron site occupancy: Mineralogy and crystal chemistry. *American Mineralogist*, **92**, 1464−1473.

Bayliss, P., Kolitsch, U., Nickel, E.H. and Pring, A. (2010) Alunite supergroup: recommended nomenclature. *Mineralogical Magazine*, **74**, 919−927.

Bisson, W.G. (2011) *Crystal structures and magnetism in jarosites: model kagomé antiferromagnets*. Unpublished PhD thesis, University College London, London, pp 164.

Breitinger, D.K., Krieglstein, R., Bogner, A., Schwab, R.G., Pimpl, T.H., Mohr, J. and Schukow, H. (1997) Vibrational spectra of synthetic minerals of the alunite and crandallite type. *Journal of Molecular Structure*, **408/409**, 287−290.

Brese, N.E. and O'Keeffe, M. (1991) Bond-valence parameters for solids. *Acta Crystallographica*, **B47**, 192−197.

Brown, I.D. (2002) *The Chemical Bond in Inorganic Chemistry. The Bond Valence Model.* International Union of Crystallography Monographs on Crystallography, Oxford University Press, Oxford, UK.

Brown, I.D. and Altermatt, D. (1985) Bond-valence parameters obtained from a systematic analysis of the inorganic crystal structure database. *Acta Crystallographica*, **B41**, 244−248.

Čejka, J. (1999) Infrared spectroscopy and thermal analysis of the uranyl minerals. Pp 521−622 in: *Uranium: Mineralogy, Geochemistry and the Environment*, (P.C. Burns and R.J. Finch, editors). Reviews in Mineralogy & Geochemistry, **38**. Mineralogical Society of America, Washington, D.C.

Chio, Ch.H., Shrama, S.K., Ming, Li.-Ch. and Muenow, D.W. (2010) Raman spectroscopic investigation on jarosite-yavapaiite stability. *Spectrochimica Acta*, **75**, 162−171.

Clark, R.C. and Reid, J.S. (1995) The analytical calculation of absorption in multifaceted crystals. *Acta Crystallographica*, **A51**, 887−897.

Dutrizac, J.E. and Jambor, J.L. (2000) Jarosites and their application in hydrometallurgy. Pp. 405−452 in: *Sulfate Minerals − Crystallography, Geochemistry and Environmental Significance* (C.N. Alpers, J.L. Jambor and D.K. Nordstrom, editors). Reviews in Mineralogy & Geochemistry, **40**. Mineralogical Society of America, Washington, DC.

Frost, R.L., Wills, R.-A., Weier, M.L., Martens, W. and Mills, S.J. (2006) A Raman spectroscopic study of selected natural jarosites. *Spectrochimica Acta*, **A63**, 1−8.

Gale, J.D., Wright, K. and Hudson-Edwards, K.A. (2010) A first-principles determination of the orientation of H_3O^+ in hydronium alunite. *American Mineralogist*, **95**, 1109−1112.

Gordon, S.C. (1941) Results of the Chilean Mineralogical Expedition of 1938. Part V. - Cadwaladerite, a new aluminium mineral from Cerro Pintados, Chile. *Notulae Naturae of The Academy of Natural Sciences of Philadelphia*, **80**, 1−4.

Grohol, D. and Nocera, D.G. (2007) Magnetic disorder in the frustrated antiferromagnet jarosite arising from the $H_3O^+−OH^-$ Interaction. *Chemistry of Materials*, **19**, 3061−3066.

Grohol, D., Nocera, D.G. and Papoutsakis, D. (2003) Magnetism of jarosites. *Physical Reviews*, **B67**, 064401.

Hayes, A.A. (1844) Description and analysis of pickeringite, a native magnesian alum. *American Journal of Science and Arts*, **46**, 360−362.

Hendricks, S.B. (1937) The crystal structure of alunite and the jarosites. *American Mineralogist*, **22**, 773−784.

Kubisz, J. (1968) *Rola dodatnych jonów wodorowo-tlenowych w minerałach*. Prace Mineralogiczne **12**, Polska Akademia Nauk, oddzial w Krakowie, Komisija Nauk Mineralogicznych, 75 pp.

Lager, G.A., Swayze, G.A., Loong, C.-K., Rotella, F.J., Richardson, J.W. and Stoffregen, R.E. (2001)

Neutron spectroscopic study of synthetic alunite and oxonium-substituted alunite. *The Canadian Mineralogist*, **39**, 1131−1138.

Lane, M.D. (2007) Mid-infrared emission spectroscopy of sulfate and sulfate-bearing minerals. *American Mineralogist*, **92**, 1−18.

Libowitzky, E. (1999) Correlation of O−H stretching frequencies and O−H···O hydrogen bond lengths in minerals. *Monatshefte für Chemie*, **130**, 1047−1059.

Majzlan, J., Stevens, R., Boerio-Goates, J., Woodfield, B.S., Navrotsky, A., Burns, P.C., Crawford, M.K. and Amos, T.G. (2004) Thermodynamic properties, low-temperature heat-capacity anomalies and single-crystal X-ray refinement of hydronium jarosite, $(H_3O)Fe_3(SO_4)_2(OH)_6$. *Physics and Chemistry of Minerals*, **31**, 518−531.

Majzlan, J., Glasnák, P., Fisher, R.A., White, M.A., Johnson, M.B., Woodfield, B. and Boerio-Goates, J. (2010) Heat capacity, entropy and magnetic properties of jarosite-group compounds. *Physics and Chemistry of Minerals*, **37**, 635−656.

Majzlan, J., Alpers, Ch.N., Koch, Ch.B., McCleskey, R.B., Myneni, S.C.B. and Neil, J.M. (2011) Vibrational, X-ray absorption and Mössbauer spectra of sulfate minerals from the weathered massive sulfide deposit at Iron Mountain, California. *Chemical Geology*, **284**, 296−305.

Momma, K. and Izumi, F. (2008) VESTA: a three-dimensional visualization system for electronic and structural analysis. *Journal of Applied Crystallography*, **41**, 653−658.

Murphy, P.J., Smith, A.M.L., Hudson-Edwards, K.A., Dubbin, W.E. and Wright, K. (2009) Raman and IR spectroscopic studies of alunite-supergroup compounds containing Al, Cr^{3+}, Fe^{3+} and V^{3+} at the *B* site. *The Canadian Mineralogist*, **47**, 663−681.

Nakamoto, K. (1986) *Infrared and Raman Spectra of Inorganic and Coordination Compounds*. Wiley, New York, 484 pp.

Nielsen, U.G., Majzlan, J., Phillips, B., Ziliox, M. and Grey, C.P. (2007) Characterization of defects and the local environment in natural and synthetic alunite $(K,Na,H_3O)Al_3(SO_4)_2(OH)_6$ by multi-nuclear solid-state NMR spectroscopy. *American Mineralogist*, **92**, 587−597.

Nielsen, U.G., Majzlan, J. and Grey, C.P. (2008) Identification of local environments in defect jarosite $(AFe_3(SO_4)_2(OD)_6$, $A = D_3O$, Na, K) samples by ^2H MAS NMR spectroscopy. *Chemistry of Materials*, **20**, 2234−2241.

Nielsen, U.G., Heinmaa, I., Samoson, A., Majzlan, J. and Grey, C.P. (2011) Insight into the local magnetic environments and deuteron mobility in jarosite $(AFe_3(SO_4)_2(OD,OD_2)_6$, A = K, Na, D_3O) and hydronium alunite $((D_3O)Al_3(SO_4)_2(OD)_6)$, from variable-temperature ^2H MAS NMR spectroscopy.

Chemistry of Materials, **23**, 3176−3187.

Nocera, D.G., Bartlett, B.M., Grohol, D., Papoutsakis, D. and Shores, M.P. (2004) Spin frustration in 2D Kagomé lattices: A problem for inorganic synthetic chemistry. *Chemistry − European Journal*, **10**, 3850−3859.

Palatinus, L. and Chapuis, G. (2007) *Superflip* − a computer program for the solution of crystal structures by charge flipping in arbitrary dimensions. *Journal of Applied Crystallography*, **40**, 451−456.

Palatinus, L. and van der Lee, A. (2008) Symmetry determination following structure solution in *P*1. *Journal of Applied Crystallography*, **41**, 975−984.

Petříček, V., Dušek, M. and Palatinus, L. (2006) *JANA2006. The crystallographic computing system.* Institute of Physics, Prague.

Pouchou, J.L. and Pichoir, F. (1985) 'PAP' (φ ρZ) procedure for improved quantitative microanalysis. Pp. 104−106 in: *Microbeam Analysis* (J.T. Armstrong, editor). San Francisco Press, San Francisco.

Ripmeester, J.A., Ratcliffe, C.I., Dutrizac, J.E. and Jambor, J.L. (1986) Hydronium ion in the alunite-jarosite group. *The Canadian Mineralogist*, **24**, 435−447.

Ross, S.D. (1974) Sulphates and other oxy-anions of group VI. Pp. 423−444 in: *The Infrared Spectra of Minerals* (V.C. Farmer, editor), The Mineralogical Society, London.

Sasaki, K., Tanaike, O. and Konno, H. (1998) Distinction of jarosite-group compounds by Raman spectroscopy. *The Canadian Mineralogist*, **36**, 1225−1235.

Sato, E., Nakai, I., Myiawaki, R. and Matsubara, S. (2009) Crystal structures of alunite family minerals: beaverite, corkite, alunite, natroalunite, jarosite, svanbergite and woodhouseite. *Neues Jahrbuch für Mineralogie, Abhandlungen*, **185**, 313−322.

Schulze, H. (1889) Mineralogisches aus Tarapacá. *Verhandlungen des Deutschen Wissenschaftlichen Vereines zu Santiago*, **2**, 49−60.

Serna, C.J., Cortina, C.P. and Ramos, J.V.G. (1986) Infrared and Raman study of alunite-jarosite compounds. *Spectrochimica Acta*, **A42**, 729−734.

Spratt, H.J., Rintoul, L., Avdeev, M. and Martens, W.N. (2013) The crystal structure and vibrational spectroscopy of jarosite and alunite minerals. *American Mineralogist*, **98**, 1633−1643.

Wilkins, R.W.T, Mateen, A. and West, G.W. (1974) The spectroscopic study of oxonium ions in minerals. *American Mineralogist*, **59**, 811−819.

Wills, A.S. and Harrison, A. (1996) Structure and magnetism of hydronium jarosite, a model Kagomé antiferromagnet. *Journal of the Chemical Society, Faraday Transactions*, **92**, 2161−2166.